

Phonon-assisted tunneling in asymmetric resonant tunneling structures

Jun-jie Shi^{*,1,3,a}, Barry C. Sanders^{1,b} and Shao-hua Pan^{1,2,3,c}

¹ Department of Physics, Macquarie University, Sydney, New South Wales 2109, Australia

² Institute of Physics, Chinese Academy of Sciences, P. O. Box 603, Beijing 100080, P. R. China

³ China Center of Advanced Science and Technology (World Laboratory), P. O. Box 8730, Beijing 100080, P. R. China

* On leave from Department of Physics, Henan Normal University, Xinxiang 453002, Henan, P. R. China

(July 24, 2017)

Based on the dielectric continuum model, we calculated the phonon assisted tunneling (PAT) current of general double barrier resonant tunneling structures (DBRTSs) including both symmetric and asymmetric ones. The results indicate that the four higher frequency interface phonon modes (especially the one which peaks at either interface of the emitter barrier) dominate the PAT processes, which increase the valley current and decrease the PVR of DBRTSs. We show that an asymmetric structure can lead to improved performance.

73.40.Gk, 73.50.Bk

I. INTRODUCTION

The double barrier resonant tunneling structure (DBRTS) [1] continues to attract attention both for its potential applications to electronic devices and for its value in exploring fundamental phenomena [2], including tests of electron-phonon coupling theories [3–13]. Despite extensive study of the DBRTS, challenging problems continue to exist with respect to practical applications and also for modeling the characteristics of the DBRTS [2]. Our objective here is to fully analyze the phonon-assisted tunneling (PAT) current, especially in the valley region, and to demonstrate that there can be important advantages in designing a DBRTS with an asymmetric structure. We include all of the phonon modes and provide a complete analysis of the relative importance of these modes, particularly for the asymmetric DBRTSs where a limited investigation has been performed to date [12,13]. It is important to consider all of the phonon modes when the asymmetric DBRTS is considered [14–16].

The motivations for considering the asymmetric DBRTS are the possibility for improving performance, tunability of the negative differential resistance (NDR) [17], and tuning of charge accumulation in the quantum well (QW) [18,19]. This asymmetry can be introduced by varying the material compositions in the two barriers or by creating two barriers of unequal width, and we will consider both possibilities here. Our treatment includes a detailed study of all of the phonon modes, assuming the dielectric continuum theory and incorporating the effects of subband nonparabolicity.

Our main concern is with DBRTS performance. A large NDR is particularly important for high-frequency resonant tunneling and rapid switching devices and is usually quantified by the peak-to-valley ratio (PVR) of the current-to-voltage characteristic curve. A large PVR and low valley current are desirable for most resonant tunneling diodes (RTD) device applications. Generally, PAT, $\Gamma - X$ intervalley tunneling, impurity scattering, the interface roughness scattering and the tunneling of

quasi-two-dimensional subband electron in the pseudo-triangular well in the emitter can cause the valley current [10]. For a polar semiconductor DBRTS, the effects of phonon scattering on resonant tunneling are very important and inevitable especially at room temperature. The electrons in the DBRTS may emit phonons during the resonant tunneling process. In general, the contribution by the PAT current is small compared with the coherent resonant tunneling process but can be large compared to the other contributions to current. Hence the total tunneling current density can be approximated by $J = J_c + J_p$, for J_c the coherent tunneling current density and J_p the PAT current density. Although the PAT current has been investigated theoretically [3–11,13], we provide a more rigorous investigation of electron-phonon scattering and the PAT current in general DBRTS including both symmetric and asymmetric ones, with the contribution of all of the phonon modes accounted for quantitatively. Hence the PAT physical picture is further clarified.

II. THEORY

Working within the framework of the dielectric continuum model and treating the electron-phonon interaction via the Fröhlich-like Hamiltonian, we can calculate the electron-phonon scattering rate W according to the Fermi golden rule for two cases [15]: scattering by interface phonons $W_{\text{int}}^{(i \rightarrow f)}(\vec{k}_i, E_z)$ and by confined LO phonons $W_{\text{LO}}^{(i \rightarrow f)}(\vec{k}_i, E_z)$. The scattering rate depends explicitly on the phonon occupation number N_{ph} which is temperature-dependent according to the Planck distribution [12]. As the width of the final resonant state is very narrow, the final state is treated as a completely localized state in the well [3–5,8,13,20]. We have recently presented the expressions of these scattering rates $W_{\text{int,LO}}^{(i \rightarrow f)}(\vec{k}_i, E_z)$ for both symmetric and asymmetric DBRTSs [12].

Electron tunneling in a DBRTS depends sensitively on the bias voltage V . The coherent tunneling current density J_c and PAT current density J_p are given by

$$J_c = en\langle T(E_z)v_z(E_z) \rangle \quad (2.1)$$

and

$$J_p = eN\langle W \rangle/A. \quad (2.2)$$

Here e is the absolute value of the electron charge, N the total electron number in the electron reservoir with volume Ω , $n = N/\Omega$ the electron density (assumed to be constant), $T(E_z)$ the electron transmission coefficient, and $v_z(E_z)$ the longitudinal electron velocity, A the cross-sectional area of the structure, and W the electron-phonon scattering rate [12]. $\langle \rangle$ represents averaging on quantum states.

From Eq. (2.1) we obtain [1]

$$J_c = J_{c\rightarrow} - J_{c\leftarrow}, \quad (2.3)$$

with

$$J_{c\rightarrow} = \frac{em_{\parallel}k_B T}{2\pi^2\hbar^3} \int_0^{\infty} T(E_z) \ln\{1 + \exp[(E_F - E_z)/k_B T]\} dE_z, \quad (2.4)$$

and

$$J_{c\leftarrow} = \frac{em_{\parallel}k_B T}{2\pi^2\hbar^3} \int_0^{\infty} T(E_z) \ln\{1 + \exp[(E_F - eV - E_z)/k_B T]\} dE_z. \quad (2.5)$$

Here $J_{c\rightarrow}$ ($J_{c\leftarrow}$) denotes the tunneling current density from the emitter (collector) to the collector (emitter), and $J_{c\rightarrow}$ is critical for the NDR of the DBRTS, which controls the coherent tunneling current density. E_F and $E_F - eV$ are, respectively, the local Fermi energy levels in the emitter and collector, and m_{\parallel} is the electron effective mass in the $x - y$ plane parallel to the interfaces of the DBRTS.

From Eq. (2.2) we derive

$$J_p = \frac{em_{\parallel}k_B T L_e}{2\pi^2\hbar^3} \left(\frac{m_z}{2}\right)^{1/2} \sum_{p=\nu,m} \int_{E_w + \hbar\omega_p}^{\infty} E_z^{-1/2} \times \ln\left[1 + e^{(E_F - E_z)/k_B T}\right] W_p(E_z) dE_z, \quad (2.6)$$

with L_e the emitter length, m_z the electron effective mass for longitudinal motion in the emitter, $\nu = 2, 3, 4$ the index for confined bulk-like LO phonon modes in the left-barrier, the well and the right-barrier layers, respectively, and m (1 to 8) the index for the eight interface phonon modes. The electron-phonon scattering rate in the ν^{th} layer is $W_{\nu}(E_z)$, and $W_m(E_z)$ is the scattering rate between electron and the m^{th} interface phonon mode. Explicit expresssions for $W_{\nu}(E_z)$ and $W_m(E_z)$ have been presented in our recent paper [12].

In obtaining Eq. (2.6) we have assumed $W(\vec{k}_i, E_z) \doteq W(0, E_z) \equiv W(E_z)$ and have ignored the contribution from collector-to-emitter tunneling via a phonon absorption [3–5].

Despite the apparent minor difference between Eqs. (2.4) and (2.6), simulating J_p is more costly in computer time compared to simulating J_c because $W_p(E_z)$ is more complicated than $T(E_z)$ [12]. Our calculations show that J_p mainly comes from the electron scattering by the higher frequency interface phonons (especially the interface phonons localized at either interface of the left barrier).

III. NUMERICAL RESULTS AND DISCUSSION

Numerical calculations have been performed for asymmetric and symmetric DBRTSs $\mathcal{A}(x, d)$ defined as

$$\mathcal{A}(x, d) \equiv n^+ \text{GaAs}(1000\text{\AA})/\text{Al}_x\text{Ga}_{1-x}\text{As}(30\text{\AA})/\text{GaAs}(60\text{\AA})/\text{Al}_{0.3}\text{Ga}_{0.7}\text{As}(d)/n^+ \text{GaAs}(1000\text{\AA}), \quad (3.1)$$

with $m_{\parallel} = m_z$ and equal doping concentration 10^{18} cm^{-3} in emitter and collector. The physical parameters used are the same as in [16].

Figure 1 presents the dispersion calculated from Eq. (4) of [15] for the eight interface modes of structure $\mathcal{A}(0.25, 20\text{\AA})$, which reveals that the four lower-frequency modes occupy a much narrower frequency band than the four higher-frequency modes. Moreover, the dispersion of the interface modes is significant for the case $k \leq 0.1\text{\AA}^{-1}$ and negligible for $k > 0.1\text{\AA}^{-1}$. The electron-interface-phonon coupling function $\Gamma(k, z)$ [15] is a complicated function of both z and k in a DBRTS. The $\Gamma(k, z) - z$ relation in Fig. 2 reveals the strength of the electron interaction with different interface modes peaks at different interfaces. For example, the electron interaction with mode 7 (denoted e-p(7)) peaks at the $z = 0$ and 30 \AA interfaces (i.e., either interface of the left barrier). We also find that $|\Gamma(k, z)|$ decreases rapidly as a function of k for $0 < k \leq 0.01\text{\AA}^{-1}$, slowly for $0.01\text{\AA}^{-1} < k < 0.08\text{\AA}^{-1}$, and then rapidly for $k > 0.08\text{\AA}^{-1}$ for the e-p(7) interaction. The 7th interface mode is much more important than the other modes in the asymmetric DBRTS, and the four higher-frequency modes produce intensive polarisation in the DBRTS, resulting in a significant interaction with electrons. On the contrary, the four lower-frequency modes produce a weak interaction with electrons compared with the higher-frequency modes, which can be ignored [12,14–16]. In the following calculations, we will thus only consider the contribution of the four higher-frequency modes to the scattering rate and the PAT current for simplicity.

Figure 3 shows the scattering rate W vs incident electron energy E_z for $\mathcal{A}(0.25, 20\text{\AA})$. For $n = 10^{18} \text{ cm}^{-3}$, the Fermi energy level $E_F = 42.5 \text{ meV}$ at $T = 300 \text{ K}$. We observe that the contribution due to interface phonons is larger than that due to LO bulk-like phonons for the

electron with lower incident energies. We know from the Fermi distribution function that the emitter states are appreciably populated only for $E_z \leq E_F + k_B T = 68.3$ meV (as $T = 300$ K). Hence, we can infer that the interface phonons contribute much more than the confined bulk-like LO phonons to the PAT current.

We present the electron-phonon scattering rate, including the subband nonparabolicity, as the dash-dot-dot line in Fig. 3, which shows that the subband nonparabolicity has a large influence on the electron-phonon scattering. The peak position shifts to a lower energy, and its value decreases under the influence of the subband nonparabolicity.

In the case of including subband nonparabolicity, PAT current-to-voltage curves are shown in Fig. 4 at $T = 300$ K for the structure $\mathcal{A}(0.25, 20\text{\AA})$. Figure 4(a) shows the tunneling current assisted by the four higher-frequency interface phonon modes and their sum. We can see from Fig. 4(a) that the 7th interface mode, which is localized at either interface of the left barrier, is the most important of all of the interface modes, and this result is consistent with the results shown in Fig. 2. The total interface PAT current is a complicated function of the applied voltage and has two peaks for increasing voltage. Figure 4(b) gives the confined bulk-like LO PAT current density in structure $\mathcal{A}(0.25, 20\text{\AA})$. This figure indicates that the PAT current from the LO phonons in the well is much larger than those from the LO phonons in the two barrier layers with a complicated behavior for increasing bias voltage. Figure 4(c) presents the total PAT current density including the interface and the confined bulk-like LO phonons. We can see from Fig. 4(c) that the interface PAT current is larger by one order of magnitude than the confined LO PAT current, confirming that interface-phonon scattering dominates over confined LO phonon scattering (c.f. Fig. 3). Moreover, Fig. 4(c) also shows that the total PAT current is a very complicated function of the applied voltage and has two peaks, similar to the results based on the Green function method [6]. This is completely due to the complexity of the contribution of the phonon modes to the PAT current in our DBRTS, as shown in Figure 4(a). Figure 4 also indicates that the PAT current is mainly determined by scattering between electrons and higher frequency interface phonons (especially the interface phonons localized at either interface of the left barrier), showing a clear physical picture for the PAT process in general DBRTS.

Figure 5 shows the total current-to-voltage curve at room temperature for $\mathcal{A}(0.25, 20\text{\AA})$, including coherent and PAT currents. This figure shows that PAT increases the valley current and decreases the PVR. The result shown in Fig. 5 is similar to those obtained by the Wigner function method [7] and the Wannier function envelope equation method [10].

We have also studied the current-voltage characteristics for DBRTSs $\mathcal{A}(0.3, d)$ with $d = 20, 30$ and 40\AA . The calculated results show that when the right-barrier thickness d increases, the peak current decreases, the PVR

increases, and the peak position shifts towards higher bias voltage. These three characteristics are in agreement with recent experimental results [18]. Moreover, we have also studied the current-voltage characteristics for $\mathcal{A}(x, 30\text{\AA})$ with $x = 0.2, 0.3$ and 0.4 . The calculated results show that when the Al composition x , and thus the height of the left barrier, increases, the peak current decreases, the PVR increases, and the peak position remains at the same bias voltage. These theoretical results, which show that an asymmetric DBRTS can lead to improved performance, await experimental confirmation.

IV. SUMMARY

Employing the dielectric continuum model, including all the phonon modes and treating conduction band nonparabolicity, the PAT process is investigated in detail. We show that for a DBRTS, no matter it is symmetric or asymmetric one, the four higher frequency modes, which reduce to two symmetric and two antisymmetric higher frequency modes for a symmetric structure, dominate the interface PAT process. In particular, for the interface PAT process in a symmetric DBRTS, the two symmetric higher frequency modes are most important, the two antisymmetric higher frequency modes are less important, and the two symmetric and antisymmetric lower frequency modes are negligible. The above opinion is different from that of Refs. [3–5].

In general, the confined LO phonons in the well layer are more important than those in the two barrier layers, and the four higher frequency interface modes (i.e., mode 5 to 8, especially the 7th one which peaks at either interface of the left barrier) dominates over the four lower frequency interface modes and all of the confined LO phonon modes to electron-phonon scattering and PAT current. The PAT increases the valley current and decreases the PVR of DBRTS. It is worth mentioning that the mode 7 becomes the highest frequency symmetric interface mode for a symmetric DBRTS. The PAT physical picture stated in the above is useful and important for further understanding PAT process in DBRTSs and for designing better RTD devices.

Subband nonparabolicity has a significant influence on electron-phonon scattering, PAT, and the current-to-voltage characteristic of a DBRTS.

We find that the peak current is reduced, the position of peak current is shifted to a higher voltage, and the PVR is enlarged if the right-barrier width is increased when the two barriers have the same height. The peak current is reduced and the PVR is increased by suitably increasing the left-barrier height when the two barriers have the same width. An asymmetric DBRTS with a suitably designed structure has a larger PVR than its commonly-used symmetric counterpart. The results obtained in this paper are useful for analysing coherence-breaking phonon scattering and for potentially important

resonant tunneling device applications.

ACKNOWLEDGMENTS

Jun-jie Shi has been supported by an Overseas Post-graduate Research Scholarship and a Macquarie University International Postgraduate Research Award. This work has been supported by an Australian Research Council Large Grant and by a Macquarie University Research Grant. We have benefitted from many useful discussions with L. Tribe, E. M. Goldys, and D. J. Skellern.

- [1] R. Tsu, L. Esaki, *Appl. Phys. Lett.* **22**, 562 (1973).
- [2] J. P. Sun, G. I. Haddad, P. Mazumder, J. N. Schulman, *Proc. IEEE* **86**, 641 (1998).
- [3] P. J. Turley, S. W. Teitsworth, *Phys. Rev. B* **44**, 3199 (1991); **44**, 8181 (1991).
- [4] P. J. Turley, S. W. Teitsworth, *J. Appl. Phys.* **72**, 2356 (1992).
- [5] P. J. Turley, S. W. Teitsworth, *Phys. Rev. B* **50**, 8423 (1994).
- [6] N. Mori, K. Taniguchi, C. Hamaguchi, *Semicond. Sci. Technol.* **7**, B83 (1992).
- [7] R. K. Mains, G. I. Haddad, *J. Appl. Phys.* **64**, 5041 (1988).
- [8] F. Chevoir, B. Vinter, *Appl. Phys. Lett.* **55**, 1859 (1989).
- [9] N. S. Wingreen, K. W. Jacobsen, J. W. Wilkins, *Phys. Rev. B* **40**, 11834 (1989).
- [10] P. Roblin, Wan-Rone Liou, *Phys. Rev. B* **47**, 2146 (1993).
- [11] W. Cai, T. F. Zheng, P. Hu, B. Yudanin, M. Lax, *Phys. Rev. Lett.* **63**, 418 (1989).
- [12] J.-J. Shi, B. C. Sanders, S.-H. Pan, *Euro. Phys. Journal B* **4**, 113 (1998).
- [13] P. J. Turley, C. R. Wallis, S. W. Teitsworth, W. Li, P. K. Bhattacharya, *Phys. Rev. B* **47**, 12 640 (1993).
- [14] Jun-jie Shi, Shao-hua Pan, *Phys. Rev. B* **51**, 17 681 (1995).
- [15] Jun-jie Shi, Shao-hua Pan, *J. Appl. Phys.* **80**, 3863 (1996).
- [16] Jun-jie Shi, Xiu-qin Zhu, Zi-xin Liu, Shao-hua Pan, Xing-yi Li, *Phys. Rev. B* **55**, 4670 (1997).
- [17] J. Chen, J. G. Chen, C. H. Yang, R. A. Wilson, *J. Appl. Phys.* **70**, 3131 (1991).
- [18] T. Schmidt, M. Tewordt, R. J. Haug, K. V. Klitzing, B. Schönherr, P. Grambow, A. Förster, H. Lüth, *Appl. Phys. Lett.* **68**, 838 (1996).
- [19] P. Orellana, F. Claro, E. Anda, S. Makler, *Phys. Rev. B* **53**, 12 967 (1996).
- [20] M. O. Vassell, J. Lee, H. F. Lockwood, *J. Appl. Phys.* **54**, 5206 (1983).

FIG. 1. The dispersion curves of the interface modes for structure $\mathcal{A}(0.25, 20\text{\AA})$.

FIG. 2. Spatial dependence of the normalized coupling functions $(\hbar e^2/A\varepsilon_0)^{-1/2}\Gamma(k, z)$ for the structure $\mathcal{A}(0.25, 20\text{\AA})$ ($k = 0.01\text{\AA}^{-1}$). Here the numbers by the curves represent the interface-phonon frequency in order of increasing magnitude: (a) for the four lower-frequency modes and (b) for the four higher-frequency modes with the interfaces localized at $z = 0, 30, 90$ and 110\AA , respectively.

FIG. 3. The normalized electron-phonon scattering rate $W/(N_{\text{ph}} + 1)$ vs incident electron energy E_z for $\mathcal{A}(0.25, 20\text{\AA})$ at the bias 150 mV. The dashed line and dash-dot line represent, respectively, the contribution of the interface phonons and confined bulk-like LO phonons, and the solid line is their sum in the absence of subband nonparabolicity. The dash-dot-dot line is the total scattering rate including subband nonparabolicity.

FIG. 4. PAT current-to-voltage curves at room temperature for $\mathcal{A}(0.25, 20\text{\AA})$, including the subband nonparabolicity: (a) Interface PAT: the dashed line represents the 5th interface mode contribution for the tunneling current, the dash-dot-dot line for the 6th mode, the thin solid line for the 7th mode, the dash-dot line for the 8th mode and the heavy solid line is their sum. (b) LO PAT: the dashed line represents the confined LO phonon in the left barrier ($\text{Al}_{0.25}\text{Ga}_{0.75}\text{As}$) contribution for the tunneling current, the dash-dot line for the LO phonon in the right barrier ($\text{Al}_{0.3}\text{Ga}_{0.7}\text{As}$), the thin solid line for the confined bulk-like LO phonon in the well (GaAs) and the heavy solid line is their sum. (c) Interface PAT current (thin solid line), confined LO PAT current (dashed line) and their sum (heavy solid line).

FIG. 5. The total current-to-voltage characteristic curve at room temperature considering the subband nonparabolicity for $\mathcal{A}(0.25, 20\text{\AA})$. The dashed line stands for the coherent tunneling current density. The solid line is the total tunneling current density combining coherent tunneling and PAT currents.

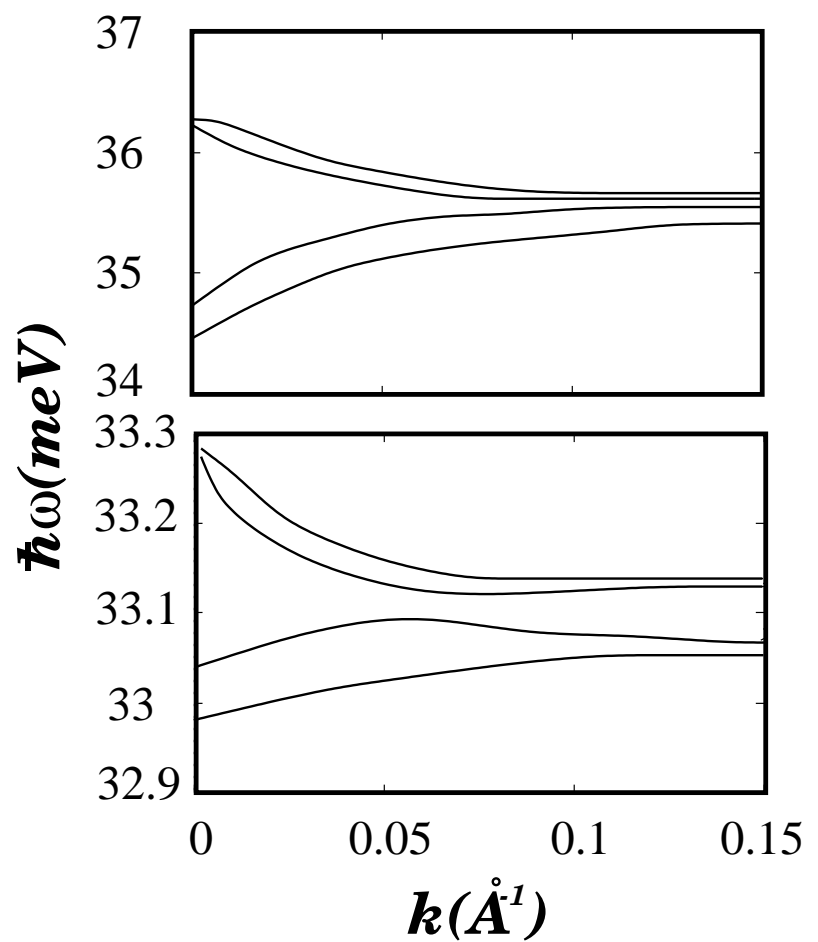


Fig. 1
Shi et al.
EPJ B

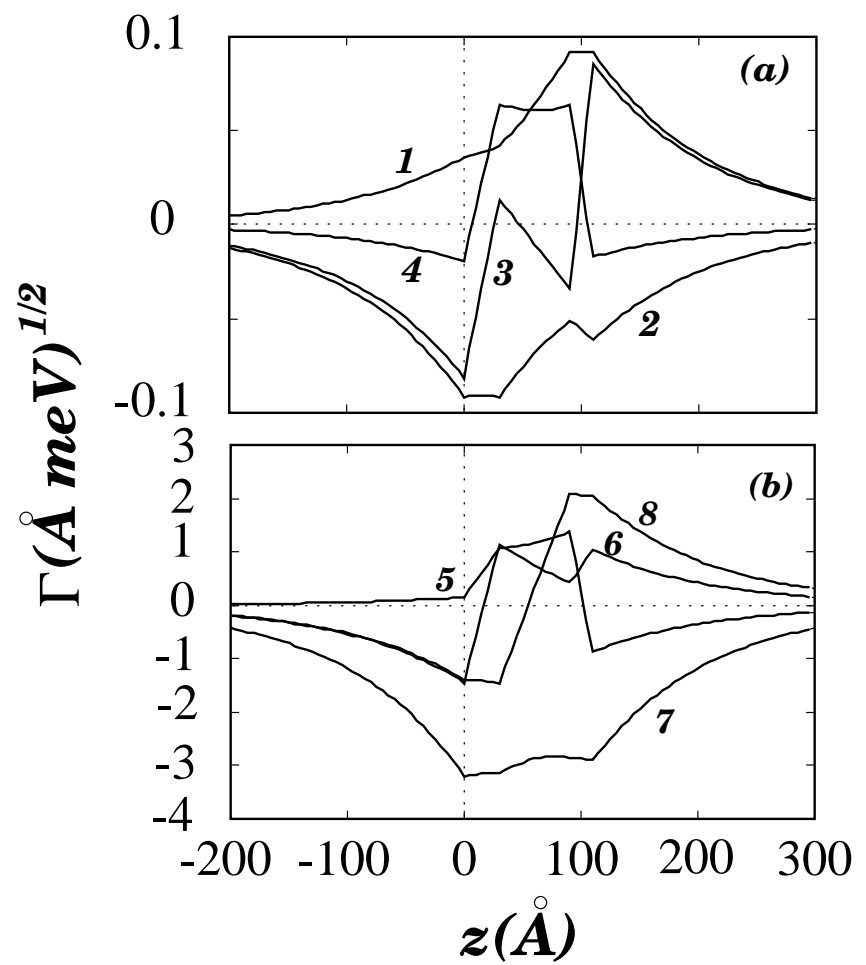


Fig. 2
Shi et al.
EPJ B

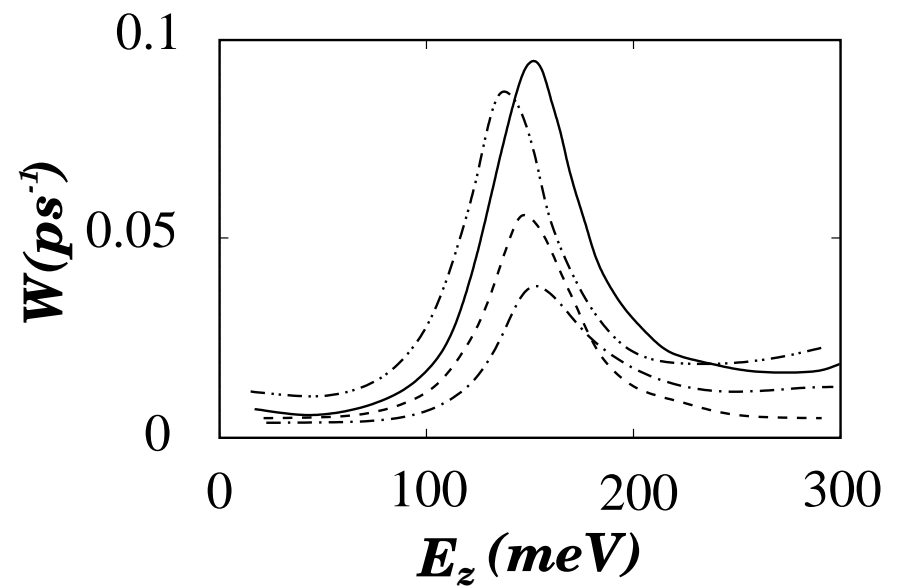


Fig. 3
Shi et al.
EPJ B

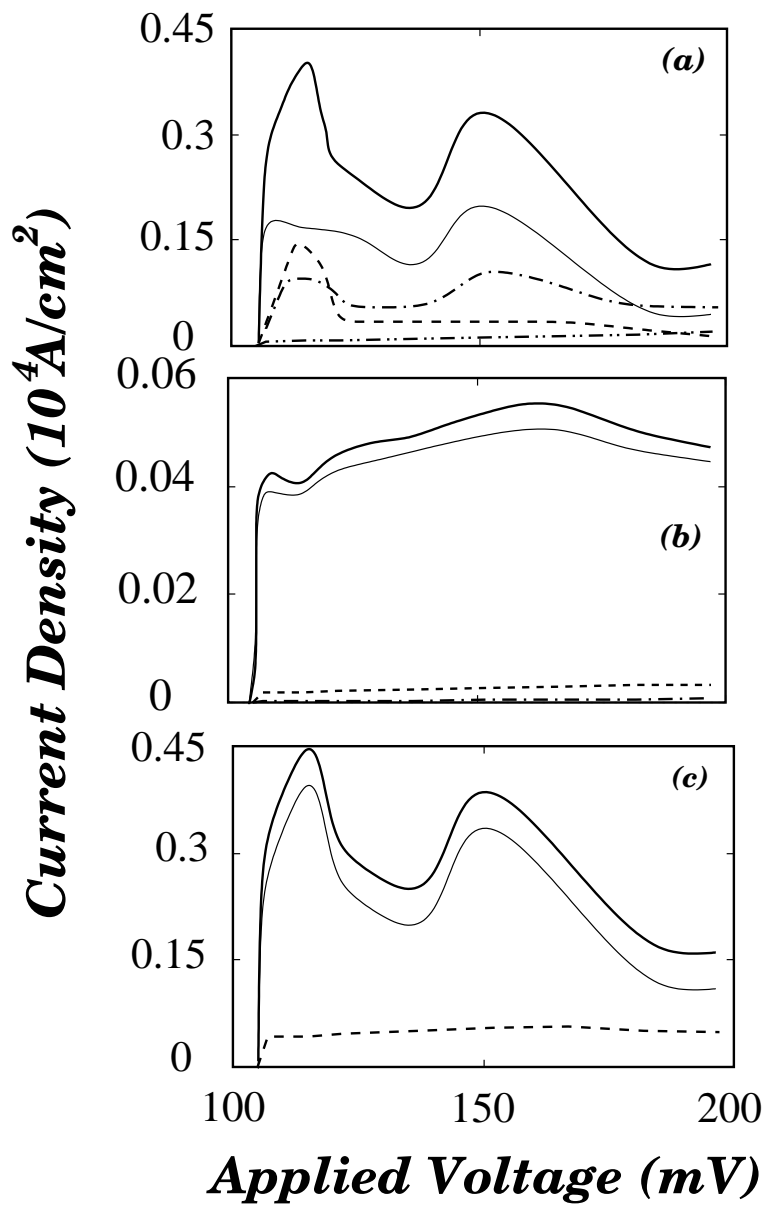


Fig. 4
Shi et al.
EPJ B

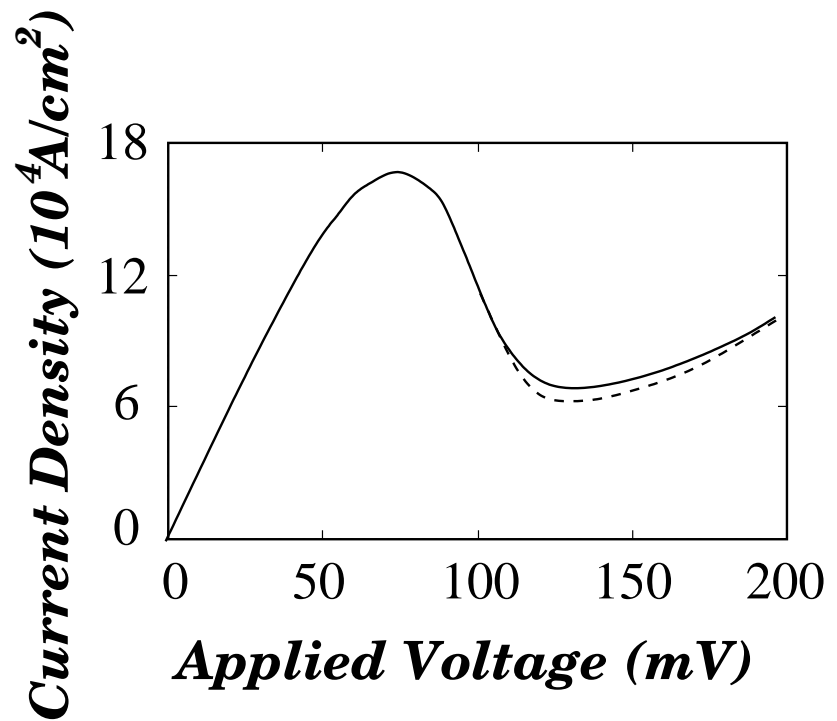


Fig. 5
Shi et al.
EPJ B